Journal of
Materials Chemistry A

Materials for energy and sustainability

Accepted Manuscript

This article can be cited before page numbers have been issued, to do this please use: C. Chowdhury, M. Lovato, G. Di Liberto, F. Viñes, F. Illas, G. Pacchioni and L. GIORDANO, *J. Mater. Chem. A*, 2026, DOI: 10.1039/D5TA07143G.

ROYAL SOCIETY OF CHEMISTRY

rsc.li/materials-a

View Article Online
DOI: 10.1039/D5TA07143G

Predicting the HER Activity of SACs on MXenes with Simple Features and Interpretable Machine Learning Models

Chandra Chowdhury,[1‡] Matteo Lovato,[1,2‡] Giovanni Di Liberto,[1] Francesc Viñes,[2] Francesc Illas,[2] Gianfranco Pacchioni,[1] Livia Giordano*[1]

[1]Department of Materials Science, University of Milano-Bicocca, Via Cozzi 55, 20125 Milano, Italy

[2]Departament de Ciència de Materials i Química Física & Institut de Química Teòrica i Computacional (IQTCUB), Universitat de Barcelona, c/ Martí i Franquès 1-11, 08028 Barcelona, Spain

Abstract

The efficient design of single-atom catalysts (SACs) for the hydrogen evolution reaction (HER) requires rapid and accurate screening methods able to handle a large number of candidate materials. Traditional density functional theory (DFT) calculations, while reliable, are computationally expensive, necessitating alternative approaches for high-throughput screening. In this work, we have created our own database based on DFT calculations using MXenes-based SACs for HER and we develop an interpretable machine learning (ML) model that predicts the hydrogen adsorption free energy (ΔG_H) with an accuracy of 0.17 eV, relying solely on simple, non-DFT-calculated features. Our approach systematically transitions from a black-box model to a grey-box model, incorporating feature importance analysis to identify key descriptors influencing ΔG_H. This ultimately leads to the development of a glass-box model, where we derive a transparent analytical equation that allows for direct prediction using raw feature values. Importantly, the final model does not require data standardization or complex computational simulations, making it highly accessible for experimental researchers and enabling rapid, first-order screening of MXene-based SACs for the HER.

‡ These authors contributed equally

View Article Online
DOI: 10.1039/D5TA07143G

Introduction

Electrochemical water (H_2O) splitting is a promising way of leveraging intermittent renewable energy to produce fuels, by forming hydrogen (H_2) and oxygen (O_2) from water. The hydrogen evolution reaction (HER), $2H^+ + 2e^- \rightarrow H_2$, represents the cathodic semi reaction of the process, which is catalyzed by Pt in commercial electrolyzers,[1-2] motivating the search for earth-abundant and cost-effective alternatives with equal (or better) electrocatalytic activity.[3-7] The equilibrium potential of this reaction is formally null, although in practice an overpotential is observed primary depending on the ability of the electrode material to bind the reaction intermediate, which is typically an adsorbed hydrogen atom, denoted as H*.[8-9] From a computational perspective, the seminal works of Nørskov and co-workers[10-11] provided an extremely successful and a handy proxy to predict the catalytic activity for HER by a descriptor consisting in the Gibbs free energy of the reaction intermediate H* (ΔG_H). The closest ΔG_H to zero, the lower the predicted overpotential is. As for example Pt(111) and other Pt-group metals show ΔG_H close to zero when dispersion corrections are included and reveal optimal performance for HER.[12] The success of this simple framework has stimulated an explosion of theoretical studies based on the screening of several catalysts toward zero overpotential.[13] This is particularly the case in the field of single atom catalysts (SACs).[14-16]

SACs have received great attention in the last years, due to their potential to reduce the amount of critical raw metal loading and to improve the catalytic activity and selectivity.[17-18] SACs are made by transition metal atoms atomically dispersed in a solid matrix, maximizing the utilization of the active phase.[19] Also, the catalytic activity of SACs can be tailored and eventually engineered by playing with the nature of the support and the local coordination of the metal atom.[20] The typical supporting matrixes are oxides and 2D materials, most often involving carbon-based supports such as graphene, N-doped graphene, and carbon nitride.[21] In recent years, MXenes, a new family of 2D materials,[22] attracted attention as supporting

View Article Online
DOI: 10.1039/D5TA07143G

templates of SACs to catalyze a variety of reactions including HER.[23-28] MXenes are two-dimensional (2D) transition-metal carbides, nitrides, and carbonitrides, and are promising in electrochemistry thanks to their electronic conductivity and ability to anchor metal atoms, and eventually to host alkaline metals in accumulators.[22, 29-30]

MXenes are synthesized from MAX phases, a material family with the general formula $M_{n+1}AX_n$ (n = 1−3), where M, A, and X correspond to early *d*-transition metals, main group *p*-elements, and C and/or N, respectively. Starting from these materials, MXenes can be obtained by selective chemical etching of the A element.[29, 31] Using selective etchants, it is possible to break the M−A bonds which are weaker than the M−X bonds resulting in highly active MXene sheets. Depending on the etchants and the subsequent chemical treatment, the thus obtained MXene sheets might be terminated with surface groups such as fluorine (−F), hydroxyl (−OH), hydrogen (−H), or oxygen (−O).[29, 32] By selecting the M and X elements, the number of atomic layers in the sheet, and the type of surface terminations, a huge number of possible MXene based material can be synthetized, opening the possibility to customize their properties.[31, 33] Additionally, recent work has shown that the surface termination can be removed or substituted in a rational, predetermined way.[34-36] Recently, Oschinski *et al.*[37] used density functional theory (DFT) to study the interaction of first row transition metals with M_2C (M = Ti, Zr, Hf, V, Nb, Ta, Cr, Mo, and W) with the aim of providing a rational guide to the design of new SAC catalysts based on MXenes and facilitate the experimental work to synthesize stable systems.

The improvement of computational power is promoting computational (electro)catalysis studies towards an even more ambitious goal, the development of descriptors and data-driven statistical models for the predictions of the catalytic activity.[38-39] In the case of HER, it translates in seeking models able to predict ΔG_H based on a set of defined physical properties (features) of the catalyst. Nevertheless, there are multiple ways to pursuit this goal, and one can adopt different data-driven approaches to find relevant correlation between the

View Article Online
DOI: 10.1039/D5TA07143G

target variable (ΔG_H) and a number of features of varied complexity. The drawback of this approach is that it typically results in a complex mathematical expression of ΔG_H as a function of the input variables, where the functional form is difficult to interpret in physical or chemical terms, and the input parameters often require the full DFT calculations of adsorbed H to be determined, raising some questions on the real predictive power of the schemes and their usefulness. There are several recent studies showing the usefulness of machine learning models for the predictive performances several electrocatalytic applications which are based on MXene systems.[40,41] For instance, Zhang *et al.*[40] utilized a high-throughput screening approach combined with a machine learning (ML) model to predict hydrogen binding energy and then the HER activity of a total of 299 MXene materials. Their methodology incorporated features such as the *d*-band centre and Bader charges, which necessitate DFT calculations of H adsorbed on the active site, and found that random forest algorithm predicts hydrogen binding energy with a root mean square error of 0.27 eV. Likewise, Umer *et al.* incorporated a comprehensive set of 29 features in their study of rationally designed 364 catalysts by embedding 3*d*/4*d*/5*d* TM single atoms on diverse substrates like graphitic carbon nitride (g-C_3N_4), π-conjugated polymer, pyridinic graphene and hexagonal boron nitride, including complicated descriptors such as the Coulomb matrix. Additionally, they integrated DFT-derived features to further refine their predictive model.[40] At this stage, we recognize a gap in the availability of a straightforward and interpretable model that relies solely on simple features. Such a model should provide a clear, user-friendly equation for predicting the target using raw feature values, without the need for data standardization. This would enable broader accessibility, allowing anyone to utilize the derived equation for initial screening with ease.

In this work we performed a computational screening of MXenes-based SACs for HER with the aim of providing a straightforward and interpretable model for the prediction of ΔG_H from simple variables that do not require any DFT calculations of the SAC or hydrogen

View Article Online
DOI: 10.1039/D5TA07143G

adsorption on the SAC. We have expanded the dataset of transition metal SACs anchored on bare MXenes (M = Ti, V, Zr, Nb, Mo, Hf, Ta, and W), from first-row transition metals reported in Ref. [37], to the second and third row, using the complete set of transition metals as SACs. We then considered the hydrogen adsorption on the resulting SACs obtaining a data set of 208 ΔG_H values. We trained statistical models with different number of features and levels of complexity to predict ΔG_H, by keeping close attention to the simplicity of the descriptors and the interpretability of the model in physically meaningful terms. We began with a black-box model and gradually transitioned to a grey-box approach[41] by conducting feature importance analysis across models ranging from linear to complex which essentially provides us the reason behind the performances of different models. Ultimately, we developed a glass-box model[41] by formulating a simple equation for the target using the interpretable and meaningful attributes, relying solely on non-DFT calculated features. Our results show that it is possible to predict a target variable with a linear multivariate model based on tabulated or easy to get features with a reasonable accuracy (about 0.17 eV), without the need to invoke complex models or not easily interpretable features. Please note that we do not claim this as the first or only interpretable model; instead, we emphasize its significance as a physically grounded, computationally efficient surrogate that connects chemical intuition with data-driven learning. The provision of a comprehensive analytical expression (Eq. 5), necessitating no preprocessing or scaling, aims to improve accessibility for researchers, especially in experimental contexts where implementing complete ML pipelines may be impractical.

The results of this study could provide a first-order screening of MXenes-based SACs for HER, aimed at identifying promising candidates for more elaborate calculations, including electronic structure and geometrical relaxation and other effects such as multiple hydrogen loading, solvation, pH and applied voltage, to then guide the experimental synthesis and characterization. We remark that the present calculations were conducted using bare M_2C

View Article Online
DOI: 10.1039/D5TA07143G

(0001) MXene surfaces, which serve as an idealized structural model. Under experimental conditions, MXenes are generally terminated with surface anions such as –O, –OH, or –F, or a mixture of them,[42] depending upon the synthesis and etching methods employed. These terminations can partially passivate the surface, hence reducing the metal binding strength compared to the uncoated surface. We chose to work with bare surfaces due to the need of identifying inherent trends in metal–support interactions and to maintain uniformity across various MXene substrates. While absolute binding energies may be reduced, the comparative trends and feature-property correlations established herein are anticipated to remain valid. Future study of this research will incorporate terminated MXenes to specifically assess the impact of surface functionalization on single-atom stability and hydrogen adsorption energetics.

Computational details

We performed DFT calculations as implemented in the Vienna *ab initio* simulation package (VASP).[43-45] We employed the Perdew−Burke−Ernzerhof (PBE) exchange-correlation functional within the generalized gradient approximation (GGA) family,[46] known to duly described metallic systems,[47-48] as most pristine MXenes are.[49] Dispersion contributions have been introduced using the D3 Grimme's procedure.[50] The Kohn−Sham equations have been solved by using an expansion of the valence electron density in a plane-wave basis set with a kinetic energy cutoff of 400 eV, whereas the effect of the core electrons on the valence density was accounted for through the projector augmented wave approach (PAW).[51-52] The energy threshold for electronic self-consistency was 10^{-6} eV, while the geometry optimizations were considered converged when the forces acting on the nuclei were all below 0.01 eV/Å. Structure optimizations were performed on a $p(3\times3)$ slab supercell, which guarantees a separation

View Article Online
DOI: 10.1039/D5TA07143G

between absorbed adatoms of ~10 Å, large enough to avoid interactions between adatoms on periodically repeated adjacent cells. The Monkhorst−Pack **k**-points sampling grid was set to 5×5×1 to perform the necessary numerical integrations in the reciprocal space.[31] A vacuum region of 16 Å is included along the c direction, in order to avoid interactions between repeated MXenes in direction perpendicular to the basal plane. We have considered the magnetic ordering in their most stable form similar to previous work.[53-54] In most of the cases the most stable form is the ferromagnetic one except Ti_2C, Hf_2C, and Zr_2C where these are in their antiferromagnetic ordering. The net charges on the atoms have been calculated by means of the quantum theory of atoms in molecules (QTAIM) developed by Bader.[55-58]

MXenes with the M_2C stoichiometry, hence with three atomic layers and exhibiting the (0001) surface, have been modelled by fully optimizing the atomic structure of the supercell representing the nanosheets with the previously optimized lattice parameter.[37] Thus, the atomic coordinates of the nanosheet atoms with the adsorbed TM atom were all fully relaxed. For the bare MXene, the atomic structure of the supercell, is as in primitive unit cell. We calculated the binding energy of anchoring transition metal (TM) adatoms as:

$$E_b = E_{SAC} - E_s - E_{TM} \quad (1),$$

where E_{SAC} is the total energy of the MXene sheet with the TM adatom attached, E_s is the total energy of the bare MXene support, and E_{TM} is the total energy of an isolated TM atom which are considered in the gas phase calculated from the DFT ground state energies. The binding energy of a metal atom to the support is a relevant quantity as it can used as a proxy of the stability of the SAC.[59] We calculated the hydrogen adsorption energy as:

$$\Delta E_H = E_{H*} - E_{SAC} - \frac{1}{2}E_{H_2} \quad (2),$$

where E_{H*} is the total energy of the system with the absorbed hydrogen atom, and E_{H_2} the energy of an isolated H_2 molecule. ΔG_H was determined from ΔE_H by adding the zero-point energy contribution and entropy terms. The entropy term involves the vibrational contribution of the adsorbed hydrogen atom including the SAC vibrational degrees of freedom and that of the gas phase hydrogen molecule, the later taken from thermodynamic tables.[10] Note that this is an approximate method to estimate the hydrogen adsorption free energy since, for instance, solvent effects are neglected. Nevertheless, the aim of this study is precisely to predict this approximate value representing a reasonable accurate estimate of ΔG_H without requiring carrying out the DFT calculations.

We employed permutation feature importance analysis for feature selection and established a Pearson correlation for the considered features. We also employed various supervised machine learning techniques to predict the features, including traditional multiple linear regression (MLR), Ridge Regression (RD), LASSO, random forest models (RF), Extra Trees (ET), Decision Trees (DT), Gradient Boosting (GB), Extra Gradient Boosting (XGB) and AdaBoost (ADB). To elucidate the validation strategy concerning the generalization capacity of our ML models, we implemented a careful data splitting approach. Initially, we randomly partitioned 15% of the full dataset as a strict external test set, entirely removed from any aspect of model training, scaling, or feature analysis. The external test set (15% of the full dataset) was extracted once at the beginning of the workflow using a fixed random seed for reproducibility. This held-out subset was kept constant and used consistently across all machine learning models. This ensured that all performance comparisons were made on the same test data, providing a fair and controlled evaluation of generalization performance. The remaining 85% of the data was subsequently used for training and validation. All model development excluding the leave-one-out procedure was performed exclusively on the 85% of the data using 10-fold cross-validation. All data preprocessing, including feature scaling using

View Article Online
DOI: 10.1039/D5TA07143G

StandardScaler within the *Pipeline*, and model fitting, was conducted solely on the training set within the cross-validation loop. The identical scaling values were utilized for the validation fold and external test sets to prevent leaking. Furthermore, for tree-based models (e.g., RF, GB), we avoided any early stopping or information leakage from the test set by depending exclusively on internal splits or designated validation subsets. For models that facilitate internal validation (e.g., GB), the validation_fraction was confined to the training set exclusively. In the leave-one-out procedures, the training set for each excluded support or metal was fixed and included all remaining data. Although the held-out subset remained fixed in each case, the models were retrained with internal randomization (e.g., bootstrapping, feature selection), leading to slightly different predictions across runs. The reported error values reflect the average across these 1000 randomized training iterations. We used a ten-fold cross-validation method with a fixed random seed (*seed* = 42) to provide a fair and robust evaluation as well as to prevent the overfitting of our model. Mean absolute error (MAE) was used as a metric for the ML models. MAE defines the average magnitude of errors predicted by our ML model with that of the predicted values from our DFT calculations. For all the ML models training and testing calculations we used the Scikit-learn library.[60] The importance analysis was based directly on the intrinsic parameters of each model type, rather than on permutation scores. For linear models (LR, RD, LASSO), we calculated importance using the absolute standardized regression coefficients, which measure each descriptor's contribution to the target following feature scaling. For tree-based and ensemble models (Decision Tree, Random Forest, Extra Trees, Gradient Boosting, AdaBoost, and XGBoost), we utilized the inherent mean decrease in impurity (MDI) values, which indicate the average variance reduction related to each feature across all decision nodes. To guarantee robustness, all importances were averaged across 100 randomized 80/20 train-test splits and normalized for each model prior to aggregation.

Results and discussion

View Article Online
DOI: 10.1039/D5TA07143G

Data set of MXenes-based SAC and their computed HER activity

We created a database of 208 SACs made by 26 TMs anchored to eight bare M_2C (0001) MXene surfaces. Figure 1 shows the binding energies and Bader charges for the TM atoms and supports considered in this study. We selected about 200 systems since it represents an acceptable size of the database to provide statistically meaningful results. Starting from the data in Ref. [37], which focused on the interaction between first-row transition metals and MXenes substrates, we expanded the calculations to the TMs of the second and third row. In this study, the adsorption stability of transition-metal atoms on MXene substrates was evaluated based on the calculated binding energy, E_b, where negative values indicate exothermic adsorption and thus stable anchoring of the metal atom. Accordingly, only systems exhibiting negative binding energies ($E_b < 0$) were considered thermodynamically stable and retained in the dataset. In contrast, combinations yielding positive or near-zero binding energies ($E_b \geq 0$) were classified as unstable, as they represent endothermic adsorption processes and weak metal–surface interactions. For Zn, Cd, and Hg, several MXene combinations produced such positive or marginal binding energies confirming negligible binding. These systems were therefore excluded from further analysis to ensure that the database and subsequent machine learning models are constructed exclusively from energetically and structurally stable SAC configurations.

View Article Online
DOI: 10.1039/D5TA07143G

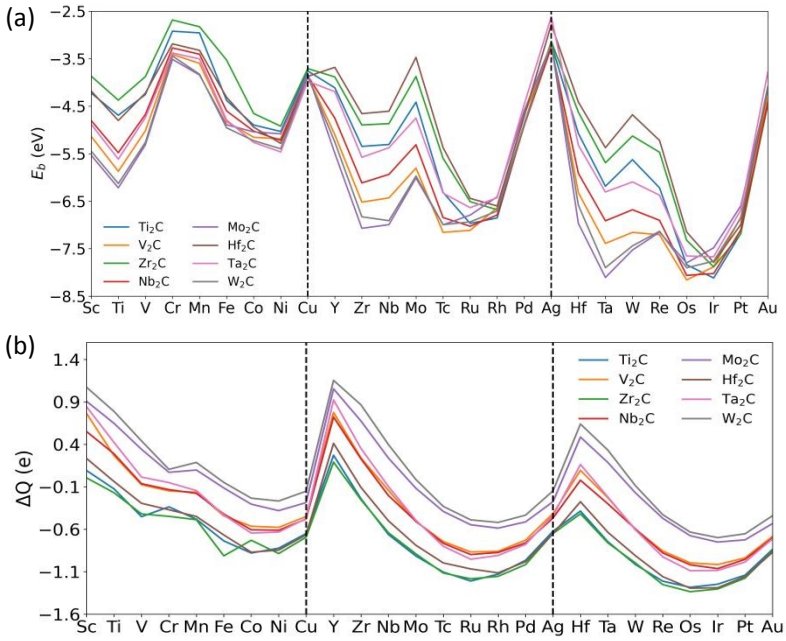

Figure 1. Properties of MXenes-based SACs. *Binding energies E_b (a) and Bader charges ΔQ (b) of transition metal atoms (TM = Sc, Ti, V, Cr, Mn, Fe, Co, Ni, Cu, Y, Zr, Nb, Tc, Mo, Ru, Rh, Pd, Ag, Hf, Ta, W, Re, Os, Ir, Pt and Au) on M_2C (0001) MXenes (M = Ti, V, Zr, Nb, Mo, Hf, Ta, and W). Vertical lines separate the three transition metal series.*

The interaction of the different first-row adatoms on each of the MXene surfaces considered has been investigated by considering the preferred adsorption sites found by Oschinski *et al.*[37] Regarding the second and third TM rows atoms, we investigated four different high symmetry sites: the atop site (T) where the adatom is placed directly above an M surface atom, the bridge site (B) corresponding to the midpoint of the M−M bond, and two hollow sites that correspond to carbon (*hcp*) and empty (*fcc*) sites, (see Figure S1 of the Supporting Information - SI). After geometry optimization, we found that the *hcp* and *fcc* sites are preferred in most cases, regardless of the adatom or substate. We found that metal adsorption is favourable for all systems considered, with binding energies ranging from -2.6 to -8.2 eV as shown in Figure 1a. As already discussed in Ref. [37] the energetic trends depend not only on the adatom but also on the MXene substrate, Figure 1a. Three similar patterns are

View Article Online
DOI: 10.1039/D5TA07143G

observed for the three TM rows (3*d*, 4*d*, 5*d*), with a W-shaped behaviour consisting of two local minima and three local maxima for the binding energy, known to be related to the special stability of d^5 and d^{10} transition metals in vacuum.[61-62] Moving along each of the series (Sc-Cu, Y-Ag, Hf-Au), the value of E_b decreases until the first minimum (Ti, Zr/Nb, Ta), then it starts to increase reaching the first maximum (Cr/Mn, Tc, W/Re, which have a half occupancy of the *nd* shell). E_b then decreases reaching the second local minimum (Ni, Ru, Os/Ir) and finally increases to reach the second maximum (Cu, Ag, Au, which have a full occupancy of the *nd* shell). In other words, elements with near half or filled *nd* shell are characterized by a weaker interaction with the surface. The effect of the substrate can be observed as a shift of the values of E_b which follow the same pattern along the series. In every series, this effect is more marked in the early elements of the row, where the E_b differences between the same TM in different substrates are more pronounced and can reach several eV, while for the late elements of the row the effect of the substrate is less noticeable, typically within 1 eV. Interestingly, the order of stability for the adsorption of the same TM atom on different substrates is maintained for the most part, with a few exceptions. In general, Mo_2C and W_2C bind the adatoms with the most negative energy values, while Hf_2C and Zr_2C form the weakest bonds. The absolute maximum values —weaker binding— for the different TM are reached for the following systems: Cr@Ta_2C, Mn@Ti_2C, Ag@Hf_2C and Ag@Ta_2C, while the absolute minimum values —stronger binding— are reached by Ru@V_2C, Os@V_2C and Ir@Ti_2C. A similar trend (especially along the 3*d* series) is observed for the average distance between TM and the three nearest neighbours (*cf.* Figure S2a), indicating that very negative binding energies correspond to small distance values.

The degree of charge transfer between the transition metal and the substrate has been analysed to gain more insight on the interactions between the TM and the eight substrates. Figure 1b reports the excess TM charge (ΔQ), calculated for the supported TM atom, obtained

View Article Online
DOI: 10.1039/D5TA07143G

from the analysis of the electron density through the QTAIM developed by Bader [55-58]. Interestingly, the same pattern is reproduced on every substrate, and a similar parabolic trend repeats for the three TM series (see Figure 1b). Another clear tendency is observed depending on the type of metal which the substrate is composed. In fact, it can be observed that charges on the adatoms adsorbed on the d^2 M_2C (Ti_2C, Zr_2C, Hf_2C), d^3 M_2C (V_2C, Nb_2C, Ta_2C), and d^4 M_2C (Mo_2C, W_2C) follow similar well-separated trends along the *d* series. Furthermore, the sign of the excess charge ΔQ depends on the type of adatom-substrate combination. For example, the values of ΔQ for d^2 M_2C substrates are negative in most cases, except for Sc and Y, Figure 1b. For d^4 M_2C the values of ΔQ are mainly positive except some exceptions, while for d^3 M_2C ΔQ values are more TM-dependent. Clearly, the oxidizing character of the d^4 M_2C MXenes is larger than that of d^3 M_2C and d^2 M_2C ones. As expected from the electronegativity trend, early TM in each d series tend to donate charge to the substrate or remain neutrals, while electrons are transferred from the substrate to late TMs, which become partially reduced.

The magnetization of the TMs anchored on MXene substrates also follow a periodic trend as shown in Figure S3 of the SI. Early and late TMs in the *d*-series expose a small number of unpaired electrons, while atoms in the middle of the series exhibit large spin values, regardless of the MXene substrate.

View Article Online
DOI: 10.1039/D5TA07143G

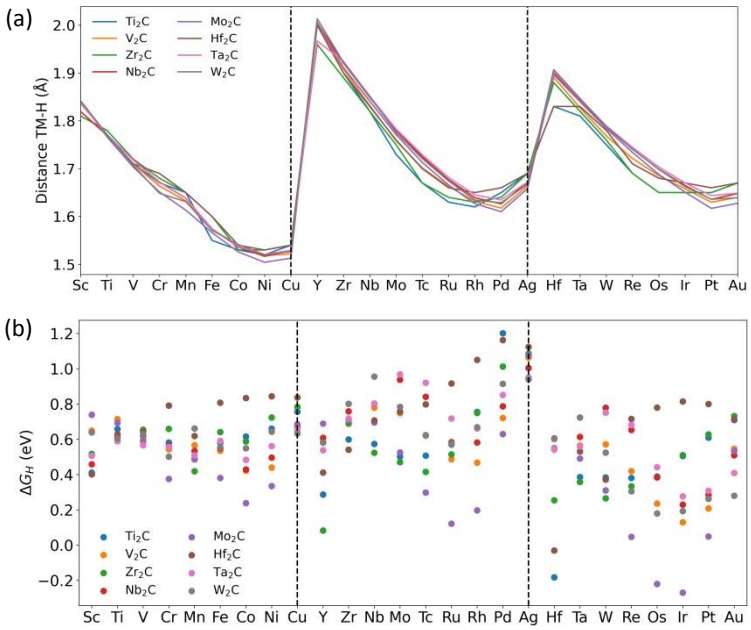

Figure 2. Hydrogen adsorption on TM@MXenes SACs. *Hydrogen-metal distances (a) and adsorption Gibbs free energies ΔG_H (b) of TM@MXenes SACs (TM = Sc, Ti, V, Cr, Mn, Fe, Co, Ni, Cu, Y, Zr, Nb, Tc, Mo, Ru, Rh, Pd, Ag, Hf, Ta, W, Re, Os, Ir, Pt, and Au; M = Ti, V, Zr, Nb, Mo, Hf, Ta, and W). Vertical lines separate the three transition metal series.*

Once the trends in the properties of TM@MXene systems have been obtained, the adsorption free energy of H on the SAC has been considered as H* is a key intermediate in HER. For each TM@MXene a hydrogen atom was adsorbed on top of the TM. Interestingly, the optimized distances between the hydrogen adatom and the TM of the SAC follow a periodic trend, with a parabolic shape similar to the one obtained for the TM charge reported in Figure 1b. For each *d*-series the TM-H distance is the largest for the first atom in the series and then decreases, reaching a minimum for Group X metals (Ni, Pd and Pt), except for Ti_2C, Zr_2C and Hf_2C substrates where the minimum occurs earlier in the series. We also noticed a strong correlation between the TM-substrate distance before and after the adsorption of hydrogen, indicating that the adsorption of H affects the interaction of TM with the substrate similarly for all considered systems (see Figure S2 of the SI).

View Article Online
DOI: 10.1039/D5TA07143G

The obtained values for the H adsorption free energy are reported as a function of the TM, in Figure 2b. Unlike the other quantities discussed above, here it is not possible to extrapolate a specific trend or relationship with the substrates or the d-series. The energy results are distributed in a range of values between -0.3 and 1.2 eV and only for a few systems the adsorption Gibbs free energy is negative. The lack of trend of ΔG_H with the TM or the substrate opens the question of whether any physical property of the SAC can be used as a descriptor for this quantity. To address this, we are trying to design an interpretable machine learning model that utilizes simple, easily accessible features, aiming to provide a transparent and intuitive predictive framework.

Dataset distribution

An essential initial stage in constructing a reliable machine learning model for predicting ΔG_H and hence the catalyst performance in the hydrogen evolution reaction is to verify that the dataset consists of a broad spectrum of adsorption energy values. The dataset distribution of ΔG_H values is depicted in Figure 3a which exhibits a wide enough distribution of values, with the bulk of data points centred within the range of 0.4 to 0.7 eV. The general distribution of the dataset closely approximates a normal distribution. The significance of a normal distribution in machine learning model prediction lies in its ability to guarantee that the model is trained on a dataset that is both balanced and representative of a broad spectrum of potential outcomes and this is crucial for mitigating bias in the model, as it enables broader learning rather than excessive adaptation to particular data points.

View Article Online
DOI: 10.1039/D5TA07143G

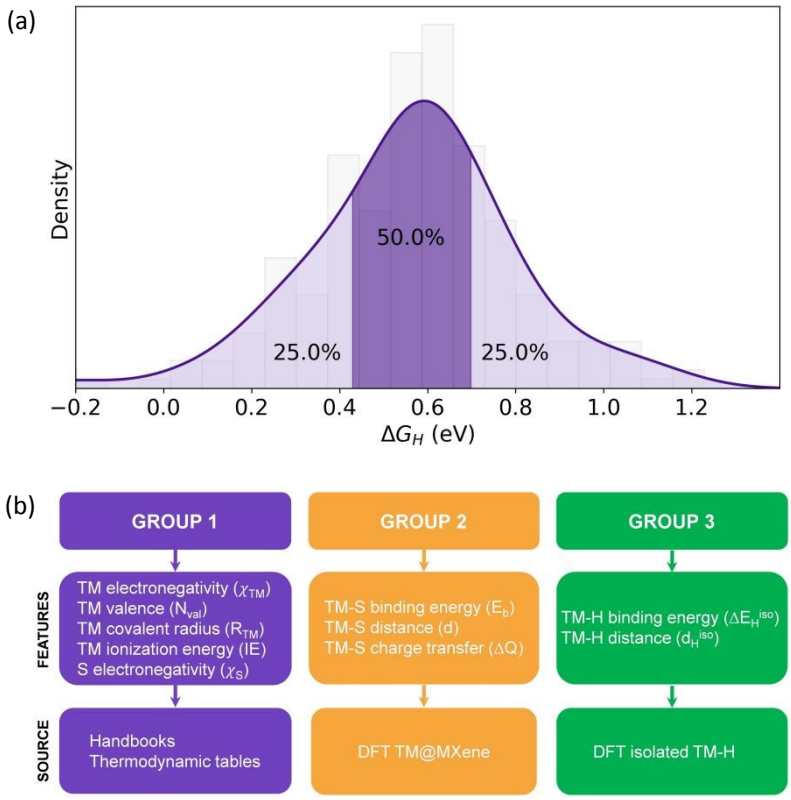

Figure 3: *(a) Data distribution plot of the target property* ΔG_H*. (b) Features of SAC systems used to build the predictive model for* ΔG_H *on MXenes based SACs: Electronegativity of the TM* (χ_{TM})*, number of TM valence electrons* (N_{val})*, TM covalent radius* (R_{TM})*, TM first ionization energy (IE), binding energy of TM to the support* (E_b)*, mean distance of TM to the support (d), Metal charge* (ΔQ)*, support electronegativity* (χ_S)*, binding energy of isolated H-TM complex* (ΔE_H^{iso})*, bond length of isolated H-TM complex* (d_H^{iso})*.*

Features selection

We have collected a number of physical properties as possible descriptors (features) of ΔG_H on MXenes based SACs. The features have been chosen with the following criteria: *i*) The descriptor should have a simple expression and be easily obtained, ideally tabulated; *ii*) the descriptor does not involve the DFT calculation of the properties of H* on the SAC, which would question its usefulness; *iii*) the property of interest should depend on a limited number of features, to avoid overfitting and to enable physical interpretation of the predictive model.

View Article Online
DOI: 10.1039/D5TA07143G

Specifically, three different groups of variables have been considered in this study, as summarized in Figure 3b.

The first group contains information describing properties of the TM constituting the SAC. The second group includes the information about the supports and their interaction with the TM. The last group accounts for the interaction of SAC with hydrogen. The features of the first group features are: the electronegativity of the TM (χ_{TM}); the number of TM valence electrons (N_{val}); the TM covalent radius (R_{COV}); the first ionization energy of the TM (IE); the electronegativity of M in the MXene substrate (χ_S). The data of this group of features are tabulated[63] and do not need any simulation. The second group contains the following features: Binding energy of TM to the support (E_b); mean distance between the adsorbed TM and the nearest neighbouring atoms of the substrate (d); Charge accumulation or depletion of the metal from the substrate (ΔQ), calculated by taking the difference between the number of valence electrons in the isolated TM atom and the number of electrons in the anchored state as provided by the Bader method. This quantity represents the charge acquired by the TM upon adsorption. The data of these features require the DFT geometry optimization of the bare MXene support and of TM adsorbed on the support. The third group of features includes: Binding energy of isolated diatomic H-TM molecules (ΔE_H^{iso}) and the corresponding bond length (d_H^{iso}). These two variables involve calculations of isolated TM atoms and their interaction with a hydrogen atom, and therefore they do not involve simulation of specific supported SACs. Considering all the three groups, we have a total of ten features for designing the model. An increase in the number of features sometimes improves the accuracy of machine learning models by supplying additional information for predictions, but at the same time it adds complexity to the model and possibly generates overfitting issues.

To check the reliability of our predictive model, we incorporated supplementary properties that, although not directly associated with hydrogen evolution activity, may

View Article Online
DOI: 10.1039/D5TA07143G

nonetheless provide significant insights. These properties encompass electron affinity, atomic mass, melting point, boiling point, the principal quantum number of the valence shell, and TM density, as it is known that in SACs the regulation of atomic density can affect the catalytic performances.[64] The resulting expanded dataset currently has a total of 16 features. We aim to compare the performance of our model utilizing both the original collection of ten features and the combined set of 16 characteristics, enabling us to assess the impact of these new properties on the model's accuracy and predictive efficacy.

Correlation among features

We first verified the correlations among the selected features. A correlation heatmap is an effective visualization technique that illustrates the linear correlations among several variables, with correlation coefficients spanning from -1 (strong negative correlation) to +1 (high positive correlation). The heatmap offers a clear and rapid visualization of feature interactions by color-coding values, usually employing red for positive and blue for negative correlations, see Figure 4a. This facilitates the identification of robust correlations, assists in feature selection for predictive models, reveals potential redundancies, and provides insight into the fundamental properties influencing system behaviours.

We notice a relatively strong relation between TMs properties in the upper-left corner (from χ_{TM} to IE), indicating that they are not completely independent. It can be also seen that ΔQ has a significant correlation with the TMs properties. Furthermore, χ_S has not significant correlations with any other variable. Similarly, the properties of the SAC@MXene, E_b and d, do not show any strong correlation between them nor with the substrate electronegativity. Finally, the properties of the TM-H diatomic molecule, ΔE_H^{iso} and d_H^{iso}, do not show any strong correlation with other properties other than a weak correlation of ΔE_H^{iso} with E_b. Metrics such as ΔQ, IE, and distance-related measures exhibit various degrees of correlation, illustrating the

View Article Online
DOI: 10.1039/D5TA07143G

complex interplay of structural, electronic, and magnetic features that affect the hydrogen adsorption energetics. The association among these properties offers insight into their combined effect on hydrogen evolution, potentially informing the selection of catalysts for enhanced performance.

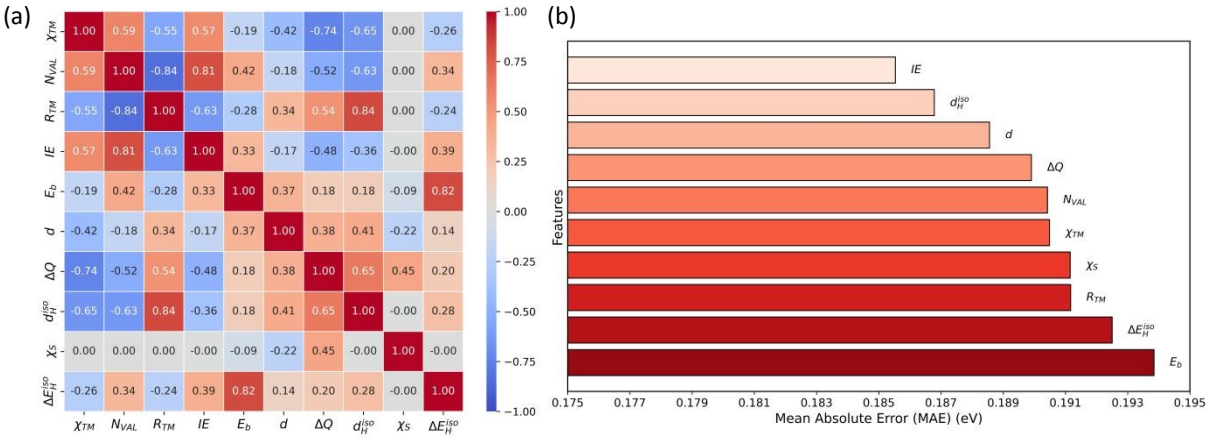

Figure 4: *(a) Correlation matrix for the features considered in this work defined in Figure 3. (b) Performance of individual features for predicting the target property, namely ΔG_H by linear regression model which is quantified as MAE. Features are ranked according to their MAE values, with lower values signifying better predictive performance.*

Linear regression with single feature

To create a straightforward, efficient model with a limited number of features capable of reliably predicting the target, we initially assessed the predictive power of each individual feature. Before designing a linear regression model, we analysed the correlation between each feature and the target variable, ΔG_H, as illustrated in the scatter plot (see Figure S4). Each column represents a distinct feature plotted against the target, utilizing raw feature values and DFT-calculated free energies to preserve analytical simplicity. The results demonstrate that individual features do not have predictive power to precisely predict the target variable. Consistently with the analysis from Figure S4, the MAE values presented in Figure 4b show that almost all features display higher MAE values (> 0.180 eV), implying limited predictive

View Article Online
DOI: 10.1039/D5TA07143G

accuracy when utilized individually. To further investigate this issue, we analysed parity plots (Figure S5 of the SI) for each individual feature, which demonstrated nearly linear trends for almost all of the features. This linearity signifies an absence of correlation between individual features and the target, hence confirming the observed high MAE values. Interestingly, few features, namely, IE, d, N_{VAL} have a lower MAE than all other features, and it also exhibits slightly better alignment (see Figure S5) with the target. Due to the lack of strong correlations between individual features and the target, as confirmed by Figure 4b and Figures S4 and S5 of the SI, it can be suggested that a multivariate regression model may be more effective in predicting ΔG_H, as it considers the combined effect of several descriptors.

Multivariate linear regression

The lack of correlation of ΔG_H with the individual physical properties suggests that one descriptor is not enough for the prediction of this quantity. A multivariate linear regression has then been performed, using the ten variables described above to predict the hydrogen adsorption free energy. The data have been standardized to take into account the different scale of the features by using the mean and standard deviation, and a set of eleven coefficients has been optimized (one for every variable and one for the constant) by minimizing the distance between a hyperplane in the variables space and our target, the H adsorption Gibbs free energy ΔG_H.

View Article Online
DOI: 10.1039/D5TA07143G

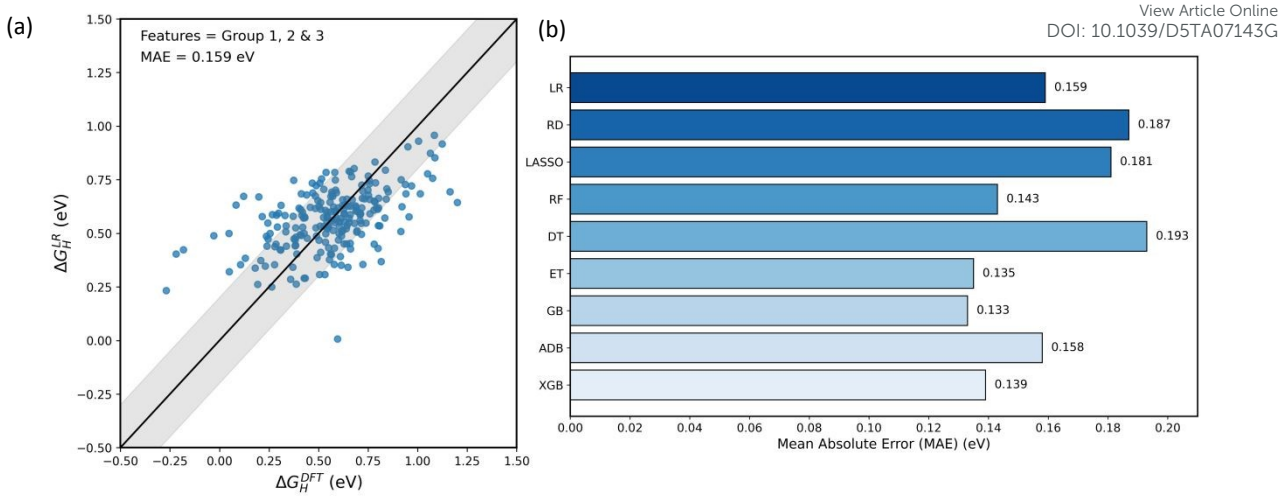

Figure 5. Multivariate linear regression. *(a) Parity plot of the multivariate linear regression for ΔG_H as a function of the features considered in this work defines in Figure 3. The shaded grey area corresponds to ±0.2 eV, which corresponds to the typical errors of DFT calculations. (b) Analysis of MAE among several machine learning models, namely, Linear regression (LR), Ridge (RD), LASSO, Extra Trees (ET), Random Forest (RF), Decision Tree (DT), Gradient Boosting (GB), AdaBoost (ADB), and XGBoost (XGB).*

The predicted values with the multivariate linear method against the original DFT data are reported Figure 5a. Overall, the model provides a MAE of 0.159 eV, which is comparable to the intrinsic error of DFT methodology. This result is quite remarkable since it indicates that calculating adsorption free energy from the multivariate linear model would not imply a reduction of accuracy. Figure 5a demonstrates the superior prediction power of the multivariate linear regression model relative to single feature based linear regression model. Although individual feature had a nearly linear, low-correlation relationship with the target variable (*cf.* Figure S5 of the SI), the integration of several features inside a linear regression framework shows a robust correlation with the target, as indicated by the close clustering of points around the parity line (see Figure 5a). The enhanced correlation indicates that the multivariable model

View Article Online
DOI: 10.1039/D5TA07143G

effectively captures complex interactions between features and the target variable, which individual features could not accomplish independently.

Comparison with complex ML models

To improve predictability, we gradually increased model complexity by exploring new methods. We assessed regularized linear models, including Ridge (RD) and LASSO, subsequently analysing tree-based models such as Random Forest (RF), Decision Tree (DT), and Extra Trees (ET). Furthermore, we evaluated boosting models, comprising Gradient Boosting (GB), AdaBoost (ADB), and XGBoost (XGB). This thorough assessment enabled us to compare the performance of these advanced models with our simple multivariate linear regression model, offering insights into the balance between model complexity and prediction accuracy. To compare the predictive power of all models, we have calculated the corresponding MAE values and the result is shown in Figure 5b. The comparison of MAE among various models illustrates the impact of model complexity on predicted accuracy. Simpler linear models, such as LR, RD, and LASSO, produce comparable MAE values ranging from 0.157 to 0.187 eV, thereby defining a baseline performance standard. The introduction of more sophisticated tree-based models yields an enhancement, especially with the ET model, which attains the lowest MAE of 0.135 eV. The RF model outperforms linear models with a MAE of 0.143 eV, while the DT shows an underperformance compared to simpler methods at 0.193 eV. Boosting techniques, such as GB, ADB, and XGB, improve accuracy, with GB attaining a notable MAE of 0.133 eV. The results indicate that models such as ET and GB offer relatively higher accuracy compared to more simplistic linear and tree-based approaches. But it is also clear that increasing model complexity does not improve the accuracy of multivariate linear models too much which signifies that our multivariate linear model is providing similar accuracy compared to the complex models.

View Article Online
DOI: 10.1039/D5TA07143G

As shown in Figure 4a, some of the tabulated transition-metal properties, particularly electronegativity (χ_{TM}), ionization energy (IE), valence electron count (N_{VAL}), and covalent radius (R_{TM}), exhibit moderate to strong pairwise correlations (~0.8), reflecting their shared periodic origin. However, the single-feature regression results presented in Figure 4b show that none of these descriptors alone can accurately predict ΔG_H (all single-feature MAEs > 0.18 eV), indicating that, despite their interdependence, they capture complementary physicochemical information rather than redundant relationships. To ensure that these correlations do not compromise model robustness, we applied regularization techniques (Ridge and LASSO regression), which constrain large coefficient magnitudes and stabilize correlated inputs. The regularized models produced nearly identical MAE values (0.16–0.18 eV) compared to the unregularized linear regression, confirming that multicollinearity does not significantly affect predictive reliability. Furthermore, to verify this conclusion, we performed an additional analysis by removing the most strongly correlated features (IE, χ_{TM}, N_{VAL}, and R_{TM}) and re-evaluated the linear regression model. The resulting MAE increased slightly from 0.159 eV (all features) to 0.179 eV (after feature removal), demonstrating that the correlated descriptors contribute synergistically to the model's predictive accuracy without introducing instability. These results confirm that the inclusion of these physically meaningful descriptors enhances the model's performance while maintaining interpretability.

Diving towards grey box model – feature importance analysis

Thus far, our methodology has predominantly depended on a black-box model, yielding predictions without an adequate understanding of the underlying factors influencing the outcomes. In order to overcome this constraint, we aim to clarify the underlying causes for the results reported across various machine learning models, from multivariate linear regression to

View Article Online
DOI: 10.1039/D5TA07143G

more complex models. We gradually transitioned from black box to grey box to simpler, interpretable glass box model as shown in a schematic diagram in Figure 6. For grey box approach we performed a feature importance analysis for each model to ascertain which features most significantly influence the predictions. This improves interpretability which will essentially bridge the gap between model's predictivity and physical understanding.

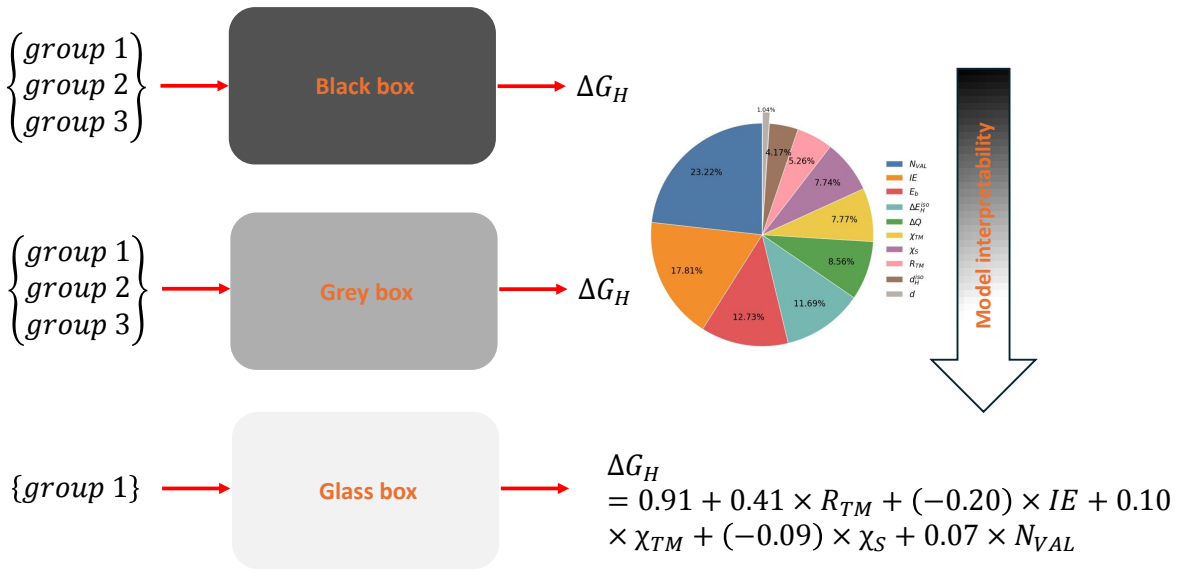

***Figure 6**: Schematic diagram for shifting from a black-box to a glass-box model for predicting ΔG_H. The black-box model produces predictions lacking interpretability, whereas the grey-box model integrates feature importance analysis to identify key contributing factors. The glass-box model simplifies the prediction process by establishing a clear equation derived from a limited number of interpretable features, hence improving transparency and usability. The downward arrow signifies the increasing interpretability of the models.*

First, we performed a feature importance analysis to further investigate the findings of the multivariate linear regression model. This is essential for identifying the features that most significantly affect the model predictions, elucidating the key factors that influence the target variable. Understanding feature importance allows us to explain the model with greater clarity and transparency. The feature importance has been evaluated by the absolute values of the

View Article Online
DOI: 10.1039/D5TA07143G

coefficients as reported in Figure 7a. Interestingly, from the feature importance analysis we found a comprehensive overview that connects the multivariate linear regression outcomes with the insights gained from individual feature performance. In the single-feature analysis, N_{VAL}, IE were identified as the features exhibiting a relatively low MAE, indicating it possessed the most robust individual correlation with the target variable. The significance of N_{VAL}, IE is further validated in the multivariate model, where it constitutes approximately 24% and 18% of the model predictive capacity, respectively, highlighting their essential function in both univariate and multivariate cases. Likewise, ΔE_H^{iso}, and χ_{TM}, which had moderate correlations in the single-feature analysis, become significant in the multivariate model. This indicates that although these features may individually possess inadequate predictive power, their synergistic effect with other factors improves the model's accuracy. The minimal contributions of the other features, in both univariate and multivariate models, indicate that they offer additional information but are not robust independent variables. This comprehensive analysis highlights the need of integrating essential features such as IE, N_{VAL}, and χ_{TM} to enhance the predictive model, utilizing their distinct and complimentary insights into the target variable.

(a)

(b)

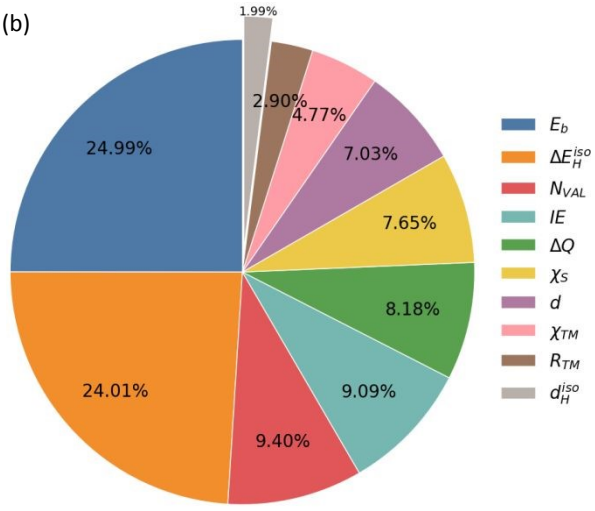

View Article Online
DOI: 10.1039/D5TA07143G

Figure 7: *(a) Feature importance analysis for multivariate linear regression (b) and Gradient Boost models.*

Similarly, to closely examine the predictive accuracy of complex models, we have performed feature importance analysis for each model and found an interesting correlation between feature distribution and model performance. For this analysis we have considered feature importance analysis for the model like GB and compared it with MLR (Figure 7b); for all other models the analysis is shown in Figure S6 of the SI. The feature importance distributions for the MLR (*cf.* Figure 7a) and GB (*cf.* Figure 7b) models illustrate the effect of increased model complexity on feature utilization and prediction accuracy. In the simplified MLR model, importance is predominantly focused on a limited number of essential features which are mainly from group 1 features, with IE, N_{VAL}, and χ_{TM} collectively prevailing, signifying a dependence on these primary descriptors. In the more complex GB model, feature importance is more evenly distributed across a broader array of all group of features, indicating that GB identifies further interactions among descriptors, utilizing a wider spectrum of information. This distributional shift corresponds to the rather superior accuracy of GB relative to MLR (MAE values 0.133 vs. 0.159 eV), demonstrating that complex models can more effectively capture nuanced patterns in the data by assigning appropriate weights to a greater number of relevant features, hence improving predictive performance.

To gain more insight from the feature importance analysis and to dive more towards grey box approach, we have created a heatmap, see Figure 8a, which provides insight into the feature importance of each model. Linear models tend to prioritize a few easily accessible features (mainly from group 2 & group 3), whereas complex models distribute importance across a wider range of features. To better understand how each model assigns importance to feature groups, we analysed the performance of each model by evaluating each group individually as shown in Figure 8b. Figure 8b presents a comparison analysis of feature group

View Article Online
DOI: 10.1039/D5TA07143G

importance across various models, demonstrating the distribution of importance among Group 1, Group 2, and Group 3 features for each model. Simple models such as LR, RD, and LASSO mostly focus on Group 1 and Group 2 features, indicating their dependence on basic properties for predictive power. With the enhancement of model complexity, tree-based models (*e.g.*, RF, ET, DT) and boosting techniques (*e.g.*, XGB, GB, ADB) tend to allocate importance more uniformly among all groups, with substantial emphasis placed on features from Group 2 and Group 3.

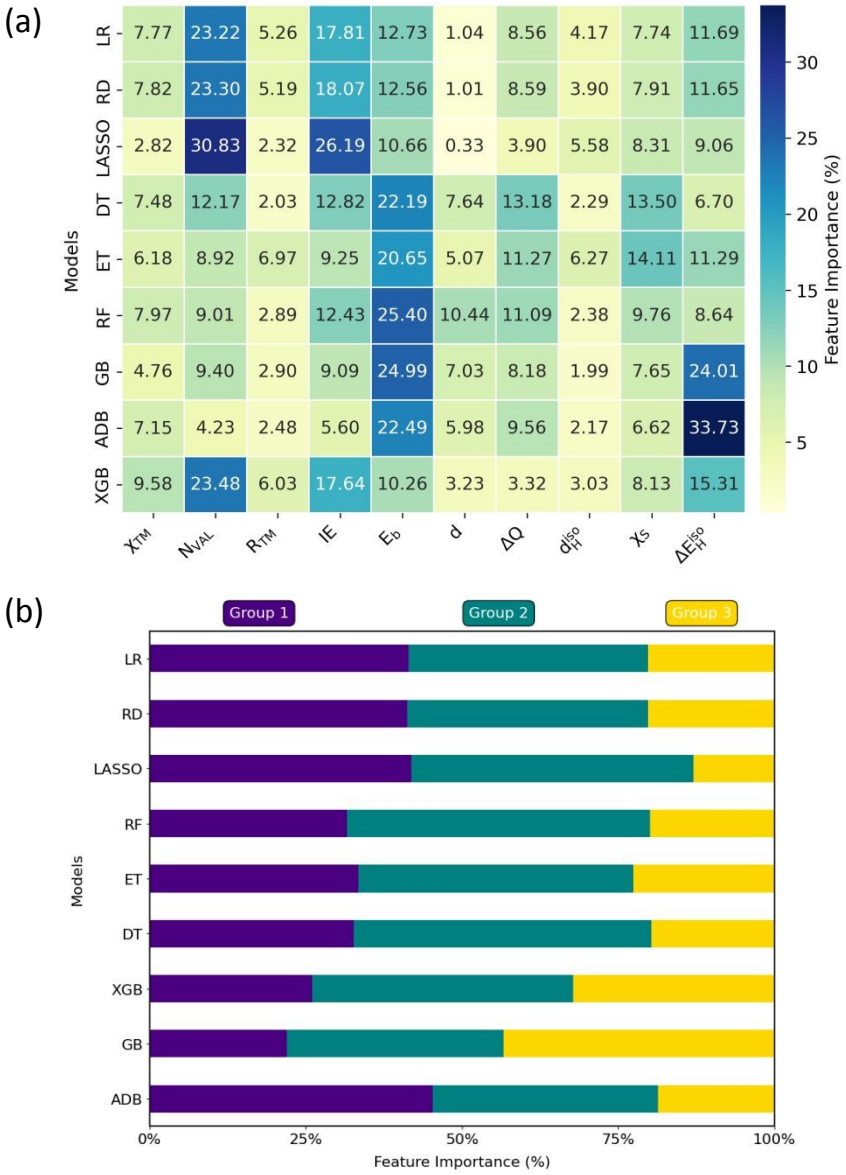

View Article Online
DOI: 10.1039/D5TA07143G

Figure 8: *(a) Heatmap illustrating feature importance for diverse models, depicting the percentage contribution of each feature to the predictions of the models. The rows denote various models while the columns specify particular features. Darker colors indicate more feature importance. (b) Feature importance distribution across different machine learning models, categorized by feature groups (Group 1, Group 2, and Group 3). The chart illustrates how simpler models, such as Linear Regression (LR), Ridge (RD), and LASSO, heavily rely on Group 1 and Group 2 features, while more complex models, including Random Forest (RF), Extra Trees (ET), and boosting methods (XGBoost, Gradient Boosting (GB), and AdaBoost (ADB)), allocate importance more evenly across all feature groups.*

This transition signifies that complex models gain from a wider range of feature interactions, compiling further information beyond the basic features in Group 1. This distributional pattern reinforces the notion that simpler models emphasize essential aspects, but more advanced models utilize a broader array of properties across groups, hence improving their capacity to identify complex interactions within the data. For all complex models, we computed the correlations between each individual group of features and the target, see Figures S6-S13 of the SI. In complex models, such as tree-based and boosting models, features from Group 2 and Group 3 demonstrate non-linear correlations with the target variable. In these models, data points are concentrated around the parity line, signifying robust prediction capability. Conversely, in linear models, the features of Group 2 and Group 3 exhibit almost linear plots (see Figure S14 of the SI) with negligible connection to the target.

Model predictive power

Since the previous sections indicate that the simpler MLR model performs quite well compared to more complex models, we focus on MLR alone to assess prediction accuracy. Once established the accuracy of the model, one needs to verify its stability and predictive power. In

View Article Online
DOI: 10.1039/D5TA07143G

order to assess the predictive power of our model we divided the data set in training and testing subsets. Three different approaches were carried out. In the first, we generated the training set by randomly extracting 75% of the original points. The coefficients of the linear model were then determined, and the model was used to predict the H adsorption energy of the remaining 25% of the dataset (testing set). That procedure was iteratively repeated 10^3 times, extracting in a random way the training and testing set. For each case, the MAE was computed and then averaged along each iteration. Remarkably, we did not observe a sizable loss in accuracy compared with the case where the entire dataset was included in the model. We found an averaged MAE of 0.16 eV, nearly unchanged from that of the original fitting, indicating a good predictive power of the model. In addition, during each iteration the regression coefficients were stored, and the mean was computed. The mean absolute deviation of coefficients was performed, and relative errors were considered to quantify the variations of the models trained with different datasets. Once again negligible changes occurred.

Next, we trained the model on a subset of the dataset, which included all data except for one support. The testing set was created using SAC supported by the newly excluded support, employing the *leave-one-out* method. The schematic diagram for this *leave-one-out* method is shown in Figure 9a for better clarity. This method enables the assessment of the model's predicted performance for each substrate without prior exposure to that particular substrate, thus evaluating the model predictive capacity across various substrates. We iterated the method for all the eight substrates for 1,000 times obtaining an averaged MAE of 0.176 eV and a maximum MAE of 0.250 eV (W_2C).

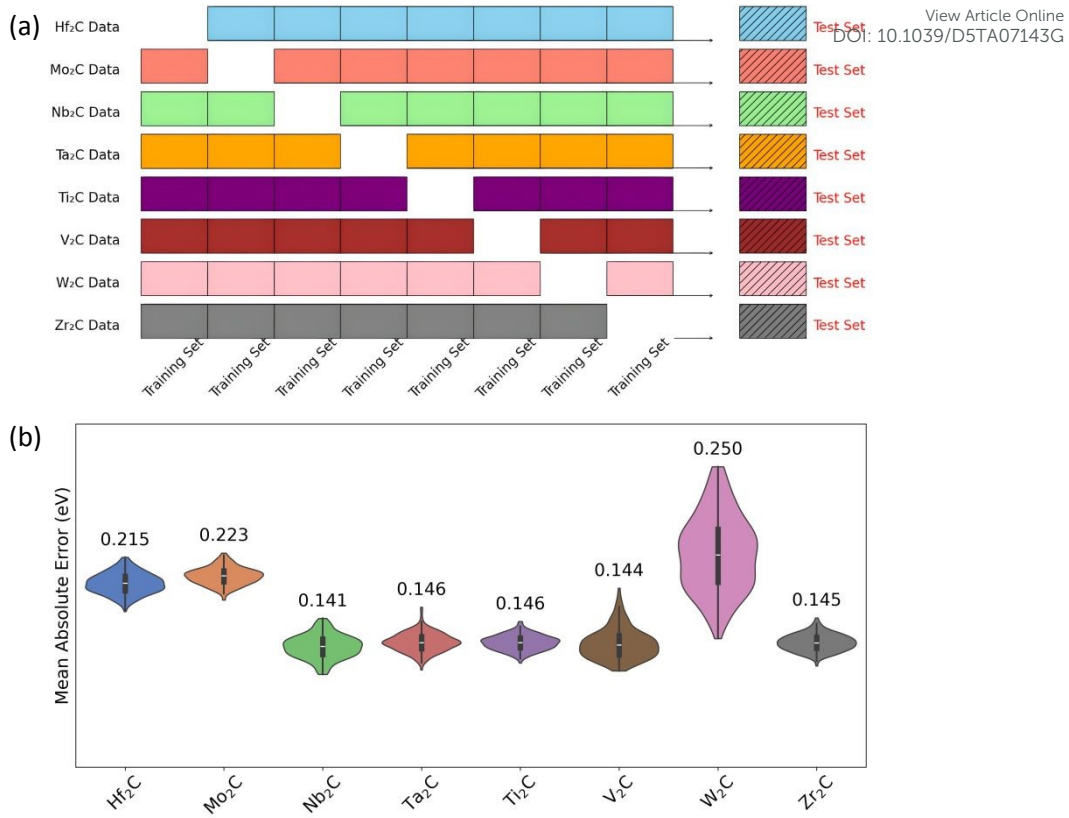

Figure 9: *(a) Scheme for the leave-one-out method employed to evaluate the predictive power of our model, wherein the data of each substrate is systematically excluded as an unseen test set, while the model is trained on the data from the other seven substrates (b) The distribution of Mean Absolute Error (MAE) for each substrate in the leave-one-out substrate experiment The violin plots illustrate the spread and central tendency of MAE values throughout 1,000 iterations, with narrower distributions signifying more consistent predictions.*

The violin plot (Figure 9b) illustrates the distribution of MAE values for each substrate across 1,000 experiments, offering insight into the variability and consistency of the model's predictions. Substrates such as Nb_2C and V_2C have low and closely grouped MAE distributions, with mean values of about 0.141 and 0.144 eV, respectively. Thus, the model predicts these substrates with precision and consistency over iterations. Conversely, W_2C and Mo_2C have relatively elevated average MAE values (0.250 and 0.223 eV, respectively) and wider dispersion, indicating reduced predictive reliability. The shape and spread of each violin

View Article Online
DOI: 10.1039/D5TA07143G

plot shows the model's stability across many substrates, with narrower distributions and lower MAEs indicating more accurate performance. To find the reason behind different prediction accuracy towards different substrates, we found that substrates like Nb_2C and V_2C have a smaller distribution of target variables (approximately 0.13 – 1.07 eV), whereas for substrates like W_2C, Mo_2C, the distributions of target variables are higher (approximately -0.26 – 1.17 eV) which might be the reason for little differences in prediction accuracy of MLR model. Finally, the same *leave-one-out* procedure was carried by including all substrates and excluding iteratively one adsorbed metal at the time, so that the model is tested on a metal single atom never seen before. The averaged MAE is 0.232 eV slightly higher than the previous cases. The corresponding violin-plot for *leave-one-out* experiment for metals is shown in Figure S15 of the SI. We observe that Ru and Rh are critical cases, as excluding them from the average calculation the MAE decreases to 0.174 eV. It is important to note that in this last assessment of the predictive power of the model the testing dataset is quite critical, only eight points, which could affect the accuracy. These assessments show the robustness and portability of the resulting model. Overall, the model can predict the hydrogen adsorption energy of unknown systems, and the method could be a starting point to screen new catalysts based on resembling substrates.

It is to be noted that to evaluate the generalization and robustness of our model, we conducted a series of validation procedures, including ten-fold cross-validation and leave-one-out tests, in which each substrate and metal were systematically excluded from training and subsequently predicted as novel systems (see Fig. 9 and SI Fig. S15). These supplementary methods guarantee that the model's predictive power is not limited to a particular subset of the dataset but encompasses various substrates and transition metals throughout the examined domain. While validation against an independent external dataset would yield the most strict assessment of transferability, such data are presently inaccessible for SAC@MXene systems

View Article Online
DOI: 10.1039/D5TA07143G

with equivalent DFT accuracy and descriptor definitions. Nevertheless, the uniform results achieved in all internal evaluations, along with the model's physically interpretable parameters, indicate its reliable applicability for screening novel and compositionally analogous systems.

Further simplifying the linear model – glass box model

We attempted to achieve our final goal of minimize the computational cost and maximize interpretability by proposing a model containing only quantities that do not involve neither the DFT simulation of H* on the SACs, as in the model discussed above, nor the SACs themself. For this reason, we have performed similar analysis by considering first only Group 1 features which essentially do not require any DFT computations.

Further we perform analysis with Group 2, Group 3 and simultaneously Group 2 & 3 features, respectively (see Figure S16 of the SI). Interestingly we found that only Group 1 features correlate nicely for the prediction of target whereas other features have poor correlation. This finding corresponds nicely with the outcomes of the feature importance analysis (*cf.* Figure 6b), which showed the considerable significance of properties like IE, N_{VAL}, all of which are classified as Group 1 features.

To construct a glass-box model, we first formulated a reduced equation by employing feature importance analysis only for Group 1 features. This method enabled us to establish a clear, interpretable connection between the chosen features and the ΔG_H target variable. The coefficients in the equation were established according to their impact on the model's predictive efficacy, ensuring that each term accurately represents the influence of its corresponding feature on ΔG_H. At first, we formulated a clear equation using all the features used in the study *i.e.* using all 10 features where the MAE is 0.16 eV and the corresponding equation is like this:

$$\Delta G_H = 1.39 + 0.78 \cdot R_{TM} - 0.74 \cdot d_H^{iso} + 0.35 \cdot \chi_{TM} - 0.29 \cdot \chi_s + 0.24 \cdot \Delta Q - 0.23 \cdot IE + 0.16 \cdot \Delta E_H^{iso} + 0.08 \cdot N_{VAL} + 0.06 \cdot d - 0.04 \cdot E_b \quad (3).$$

View Article Online
DOI: 10.1039/D5TA07143G

After that, we employed standardized features (see Figure S17a of the SI for feature importance analysis), whereby each feature was normalized to possess a mean of zero and a standard deviation of one. The simple equation is:

$$\Delta G_H = 0.91 + 0.41 \cdot R_{TM} - 0.20 \cdot IE + 0.10 \cdot \chi_{TM} - 0.09 \cdot \chi_S + 0.07 \cdot N_{VAL} \quad (4).$$

This equation offers a straightforward, interpretable, and computationally efficient method to estimate ΔG_H on SACs at the considered MXenes utilizing a small set of readily available features with a MAE of 0.17 eV (see Figure S17b of the SI for parity plot). To further simplify our model, we explored the possibility of using non-standardized features to assess the predictive efficiency while ensuring ease of application. By utilizing raw feature values, we aimed to create a model that eliminates the need for data preprocessing implying any prior standardization is not required which is important as it does not require any standardization coefficients, allowing anyone to perform an initial screening without requiring specialized programming or statistical transformations. This approach makes the model even more accessible, particularly for experimental researchers and practitioners looking for a quick and intuitive way to estimate ΔG_H. Interestingly, when we switched to non-standardized features, we observed a slight shift in the MAE values (0.18 eV, see Figure S18 of the SI for parity plot) as in the standardized case and the corresponding simplified equation is:

$$\Delta G_H = 0.34 + 0.76 \cdot R_{TM} - 0.19 \cdot IE - 0.15 \cdot \chi_S + 0.11 \cdot N_{VAL} + 0.01 \cdot \chi_{TM} \quad (5).$$

This finding is particularly valuable, as it confirms that the simplified, non-standardized model can be used directly with raw data, making it a practical tool for initial screening and decision-making in material selection. It is essential to understand that, although the glass-box model (Equations 4–5) offers a highly interpretable analytical connection grounded purely upon tabulated atomic properties, this simplification inherently imposes constraints on predicting accuracy. The parity plots (SI Figs. S17b and S18) indicate that specific systems,

View Article Online
DOI: 10.1039/D5TA07143G

especially those at the extremities of the ΔG_H range, display significant dispersion in relation to the parity line. This dispersion may result from localized geometric and electronic properties that are not explicitly captured by the basic atomic descriptors employed in this glass-box model. Nevertheless, the glass-box equation effectively captures the trends within the dataset, attaining a MAE of roughly 0.17 eV, which is analogous to the intrinsic error of DFT-calculated adsorption free energies. This accuracy is sufficient for fast, preliminary evaluation and for differentiating between distinctly promising and less effective catalyst candidates. In contrast to single-feature models (e.g., solely ionization energy or valence count) and models utilizing Group 2 or Group 3 features—which demonstrate minimal predictive capability and produce parity plots nearly parallel to the x-axis (Figs. S5, S16)—the Group 1-based model displays a distinct correlation with the DFT reference values (Fig. S18). This indicates that, despite its simplicity, the model effectively captures significant multivariate structure–property correlations. Consequently, we emphasize that the glass-box model should be considered a physically significant, predictive framework that prioritizes transparency and accessibility over high-precision quantitative estimations. This result validates the efficiency and simplicity of our model, demonstrating that precise predictions may be achieved without supplementary DFT calculations, thereby reinforcing our aim of developing a computationally efficient and interpretable model. Note also that to assess if interpretability undermines prediction performance, we compared our linear models with various sophisticated, high-capacity algorithms, including RF, ET, GB, ADB, and XGB (refer to Fig. 5b). The top-performing black-box models, including GB and ET, attained MAE values of approximately 0.133–0.135 eV, somewhat lower than the 0.159 eV produced with the multivariate linear regression model. The minor discrepancy of 0.02–0.03 eV falls within the intrinsic error of DFT-calculated adsorption free energies (about 0.10–0.20 eV), suggesting that our interpretable methodology maintains almost same predictive capability. Thus, the linear model presents an advantageous

View Article Online
DOI: 10.1039/D5TA07143G

compromise—attaining DFT-level precision while establishing transparent, physically significant correlations between descriptors and ΔG_H. This illustrates that interpretability may be achieved without much compromise in predicted performance, rendering the suggested model both scientifically accessible and computationally efficient for expedited catalyst screening.

Discussion and conclusions

Our thorough investigation has uncovered substantial insights regarding predictive performance and feature importance across various modelling methodologies. The greater accuracy of complicated models, including tree-based methods (*e.g.*, RF and ET) and boosting models (*e.g.*, GB and XGB), is due to their superior ability to utilize features from all groups of variables (Group 1, Group 2, and Group 3). These models allocate feature importance more uniformly, enabling them to identify non-linear correlations and complex interactions among many types of features. Conversely, LR focuses predominantly on Group 1 and Group 2 features, attaining prediction accuracy through a limited selection of features. The emphasis on simpler features (mainly Group 1 features) in simpler models, especially LR, is significant as these properties are easily obtainable from conventional chemistry handbooks, incurring no further computational costs. To ascertain if enhanced model accuracy could be attained through increased complexity, we combined the feature set by incorporating six additional periodic-table-derived descriptors, resulting in a total of 16 features. These were selected to preserve simplicity and universal applicability while somewhat enhancing descriptor diversity. Nevertheless, as illustrated in Figure S19, models trained on this combined feature set did not demonstrate any significant improvement in performance. The MAEs for all regressors were essentially constant, with variations of less than 0.01–0.02 eV overall. This indicates that the

primary 10 features encompass the most chemically important information for predicting ΔG_H in this dataset. It further shows the reliability of our model as well as the features.

Conversely, the properties of Group 2 and Group 3 necessitate additional DFT calculations, which may be computationally expensive, especially for large datasets. Thus, although complex models provide enhanced accuracy, they require greater processing resources owing to their dependence on features from Group 2 and Group 3. The LR model attains satisfactory accuracy while reducing computing expenses, offering an attractive trade-off between accuracy and efficiency. This trade-off indicates that, based on application requirements, the LR model may be the ideal selection for scenarios when computational efficiency is paramount.

We finally underline that the final model predicts the hydrogen binding energy with an accuracy of 0.170 eV by using only quantities that do not require any atomistic simulation of the SACs. In this respect, the model could be of help to provide a first-order approximation for the screening of SACs for HER based on M_2C like MXenes, followed by more accurate calculations on promising candidates. The MAE values for the best-performing models (0.13–0.18 eV) are comparable to the intrinsic accuracy limits of DFT, often ranging from 0.10 to 0.20 eV for hydrogen adsorption free energies, depending upon the functional and dispersion corrections employed. From a practical viewpoint, this level of accuracy suffices for initial screening of MXene-based SACs, facilitating the dependable identification of interesting candidates with near-optimal ΔG_H values (ΔG_H < 0.2 eV). The model is designed not to substitute comprehensive DFT computations but to assist in their prioritization, delivering DFT-level performance at a significantly reduced computational expense. Note also that even if the conclusions are extracted from SACs involving M_2C like MXenes, it is likely that the presented model work reasonably well for M_2C_3 and M_3C_4 MXenes, as the number of atomic layers has a small influence on adsorption properties of molecules such as CO_2.[65] Further work will be dedicated to the extension of the approach to other relevant supports.

View Article Online
DOI: 10.1039/D5TA07143G

Supporting Information

The supplementary materials contains the following: adatom adsorption sites, TM-substrate distance before and after H-binding, magnetization value of TM adsorbed on substrate, correlation with DFT-calculated features, parity plot for single variable linear regression models, feature importance analysis for different models, parity plots for different models, leave-one-out experiment with individual metals, comparison of MAE among several models utilizing 10 and 16 features.

Author information

Corresponding author:

Livia Giordano - Department of Materials Science, University of Milano-Bicocca, Via Cozzi 55, 20125 Milano, Italy. Email: livia.giordano@unimib.it

Author contributions

C.C. and M.L. contributed equally to this work. The manuscript has written with the contributions from all the authors.

Conflicts of interest

There are no conflicts to declare.

Data availability

Relevant data are available from the corresponding author upon reasonable request. The data supporting this article have been included as part of the Supplementary Information. The Supplementary Information contains the following contents: adatom adsorption sites, TM-substrate distance before and after H-binding, magnetization value of TM adsorbed on substrate, correlation with DFT-calculated features, parity plot for single variable linear

View Article Online
DOI: 10.1039/D5TA07143G

regression models, feature importance analysis for different models, parity plots for different models, leave-one-out experiment with individual metals, comparison of MAE among several models utilizing 10 and 16 features.

Acknowledgement

Access to the CINECA supercomputing resources was granted via ISCRAB. M. L. was supported in part by an Erasmus+ traineeship grant. F.V. and F.I. thank the spanish *Ministerio de Ciencia e Innovación* (MCIN) and *Agencia Estatal de Investigación* (AEI) MCIN/AEI/10.13039/501100011033 and, as appropriate, by "European Union Next Generation EU/PRTR", for grants PID2021-126076NB-I00 and PID2024-159906NB-I00, funded partially by FEDER *Una manera de hacer Europa*, as well as for the *Unidad de Excelencia María de Maeztu* CEX2021-001202-M granted to the IQTCUB. The *Generalitat de Catalunya* funding through 2021SGR00079 grant is also acknowledged. F.V. thanks the ICREA Academia Award 2023 Ref. Ac2216561.

References

1. Bockris, J.; Ammar, I.; Huq, A., The Mechanism of the Hydrogen Evolution Reaction on Platinum, Silver and Tungsten Surfaces in Acid Solutions. *J. Phys. Chem.* **1957,** *61* (7), 879-886.
2. Yu, Z. Y.; Duan, Y.; Feng, X. Y.; Yu, X.; Gao, M. R.; Yu, S. H., Clean and Affordable Hydrogen Fuel from Alkaline Water Splitting: Past, Recent Progress, and Future Prospects. *Adv. Mater.* **2021,** *33* (31), 2007100.
3. Jaramillo, T. F.; Jørgensen, K. P.; Bonde, J.; Nielsen, J. H.; Horch, S.; Chorkendorff, I., Identification of Active Edge Sites for Electrochemical H2 Evolution from MoS2 Nanocatalysts. *Science* **2007,** *317* (5834), 100-102.
4. Voiry, D.; Salehi, M.; Silva, R.; Fujita, T.; Chen, M.; Asefa, T.; Shenoy, V. B.; Eda, G.; Chhowalla, M., Conducting MoS2 Nanosheets as Catalysts for Hydrogen Evolution Reaction. *Nano Lett.* **2013,** *13* (12), 6222-6227.

5. Yao, S.; Zhang, X.; Chen, A.; Zhang, Z.; Jiao, M.; Zhou, Z., Algorithm Screening to Accelerate Discovery of 2D Metal-Free Electrocatalysts for Hydrogen Evolution Reaction. *J. Mater. Chem. A.* **2019,** *7* (33), 19290-19296.
6. Jiao, Y.; Zheng, Y.; Jaroniec, M.; Qiao, S. Z., Design of Electrocatalysts for Oxygen-and Hydrogen-Involving Energy Conversion Reactions. *Chem. Soc. Rev.* **2015,** *44* (8), 2060-2086.
7. Mahmood, J.; Li, F.; Jung, S.-M.; Okyay, M. S.; Ahmad, I.; Kim, S.-J.; Park, N.; Jeong, H. Y.; Baek, J.-B., An Efficient and pH-Universal Ruthenium-Based Catalyst for the Hydrogen Evolution Reaction. *Nat. Nanotechnol.* **2017,** *12* (5), 441-446.
8. Rüetschi, P.; Delahay, P., Hydrogen Overvoltage and Electrode Material. A Theoretical Analysis. *J. Chem. Phys.* **1955,** *23* (1), 195-199.
9. Vesborg, P. C.; Seger, B.; Chorkendorff, I., Recent Development in Hydrogen Evolution Reaction Catalysts and Their Practical Implementation. *J. Phys. Chem. Lett.* **2015,** *6* (6), 951-957.
10. Nørskov, J. K.; Bligaard, T.; Logadottir, A.; Kitchin, J.; Chen, J. G.; Pandelov, S.; Stimming, U., Trends in the Exchange Current for Hydrogen Evolution. *J. Elec. Chem. Soc.* **2005,** *152* (3), J23.
11. Skúlason, E.; Tripkovic, V.; Björketun, M. E.; Gudmundsdóttir, S.; Karlberg, G.; Rossmeisl, J.; Bligaard, T.; Jónsson, H.; Nørskov, J. K., Modeling the Electrochemical Hydrogen Oxidation and Evolution Reactions on the Basis of Density Functional Theory Calculations. *J. Phys. Chem. C.* **2010,** *114* (42), 18182-18197.
12. Allés, M.; Meng, L.; Beltrán, I.; Fernández, F.; Viñes, F., Atomic Hydrogen Interaction with Transition Metal Surfaces: A High-Throughput Computational Study. *The Journal of Physical Chemistry C* **2024,** *128* (47), 20129-20139.
13. Greeley, J.; Nørskov, J. K., Large-Scale, Density Functional Theory-Based Screening of Alloys for Hydrogen Evolution. *Surf. Sci.* **2007,** *601* (6), 1590-1598.
14. Barlocco, I.; Cipriano, L. A.; Di Liberto, G.; Pacchioni, G., Modeling Hydrogen and Oxygen Evolution Reactions on Single Atom Catalysts with Density Functional Theory: Role of the Functional. *Adv. Theory Simul.* **2023,** *6* (10), 2200513.
15. Gao, G.; Bottle, S.; Du, A., Understanding the Activity and Selectivity of Single Atom Catalysts for Hydrogen and Oxygen Evolution via Ab Initial Study. *Catal. Sci. Technol.* **2018,** *8* (4), 996-1001.
16. Di Liberto, G.; Cipriano, L. A.; Pacchioni, G., Role of Dihydride and Dihydrogen Complexes in Hydrogen Evolution Reaction on Single-Atom Catalysts. *J. Am. Chem. Soc.* **2021,** *143* (48), 20431-20441.
17. Wang, A.; Li, J.; Zhang, T., Heterogeneous Single-Atom Catalysis. *Nat. Rev. Chem.* **2018,** *2* (6), 65-81.
18. Yang, X.-F.; Wang, A.; Qiao, B.; Li, J.; Liu, J.; Zhang, T., Single-Atom Catalysts: A New Frontier in Heterogeneous Catalysis. *Acc. Chem. Res.* **2013,** *46* (8), 1740-1748.
19. Chen, Y.; Ji, S.; Chen, C.; Peng, Q.; Wang, D.; Li, Y., Single-Atom Catalysts: Synthetic Strategies and Electrochemical Applications. *Joule* **2018,** *2* (7), 1242-1264.
20. Yang, Y.; Liu, J.; Liu, F.; Wang, Z.; Wu, D., FeS2-Anchored Transition Metal Single Atoms for Highly Efficient Overall Water Splitting: A DFT Computational Screening Study. *J. Mater. Chem. A.* **2021,** *9* (4), 2438-2447.
21. Hossain, M. D.; Liu, Z.; Zhuang, M.; Yan, X.; Xu, G. L.; Gadre, C. A.; Tyagi, A.; Abidi, I. H.; Sun, C. J.; Wong, H., Rational Design of Graphene-Supported Single Atom Catalysts for Hydrogen Evolution Reaction. *Adv. Ener. Mater.* **2019,** *9* (10), 1803689.
22. Anasori, B.; Gogotsi, Y., The Rise of MXenes. *ACS Nano* **2019,** *13*, 8491-8494.

23. Zhang, J.; Zhao, Y.; Guo, X.; Chen, C.; Dong, C.-L.; Liu, R.-S.; Han, C.-P.; Li, Y.; Gogotsi, Y.; Wang, G., Single Platinum Atoms Immobilized On An MXene As An Efficient Catalyst For The Hydrogen Evolution Reaction. *Nat. Catal.* **2018,** *1* (12), 985-992.
24. Cheng, Y.; Dai, J.; Song, Y.; Zhang, Y., Single Molybdenum Atom Anchored on 2D Ti2NO2 MXene as a Promising Electrocatalyst for N2 Fixation. *Nanoscale* **2019,** *11* (39), 18132-18141.
25. Li, L.; Wang, X.; Guo, H.; Yao, G.; Yu, H.; Tian, Z.; Li, B.; Chen, L., Theoretical Screening of Single Transition Metal Atoms Embedded in MXene Defects As Superior Electrocatalyst of Nitrogen Reduction Reaction. *Small Methods* **2019,** *3* (11), 1900337.
26. Yang, X.; Lu, Z.; Cheng, C.; Wang, Y.; Zhang, X.; Yang, Z.; Lu, W., Identification of Efficient Single-Atom Catalysts Based on V2CO2 MXene by Ab Initio Simulations. *J. Phys. Chem. C.* **2020,** *124* (7), 4090-4100.
27. Kan, D.; Wang, D.; Zhang, X.; Lian, R.; Xu, J.; Chen, G.; Wei, Y., Rational Design of Bifunctional ORR/OER Catalysts Based on Pt/Pd-Doped Nb2CT2 MXene by First-Principles Calculations. *J. Mater. Chem. A.* **2020,** *8* (6), 3097-3108.
28. Fang, W.; Du, C.; Kuang, M.; Chen, M.; Huang, W.; Ren, H.; Xu, J.; Feldhoff, A.; Yan, Q., Boosting Efficient Ambient Nitrogen Oxidation By A Well-Dispersed Pd on MXene Electrocatalyst. *Chem. Comm.* **2020,** *56* (43), 5779-5782.
29. Naguib, M.; Kurtoglu, M.; Presser, V.; Lu, J.; Niu, J.; Heon, M.; Hultman, L.; Gogotsi, Y.; Barsoum, M. W., Two-Dimensional Nanocrystals Produced by Exfoliation of Ti3AlC2. In *MXenes*, Jenny Stanford Publishing: 2023; pp 15-29.
30. Naguib, M.; Mashtalir, O.; Carle, J.; Presser, V.; Lu, J.; Hultman, L.; Gogotsi, Y.; Barsoum, M. W., Two-Dimensional Transition Metal Carbides. *ACS Nano* **2012,** *6* (2), 1322-1331.
31. Alhabeb, M.; Maleski, K.; Anasori, B.; Lelyukh, P.; Clark, L.; Sin, S.; Gogotsi, Y., Guidelines for Synthesis and Processing of Two-Dimensional Titanium Carbide (Ti3C2Tx-MXene). *Chem. Mater.* **2017,** *29* (18), 7633-7644.
32. Hope, M. A.; Forse, A. C.; Griffith, K. J.; Lukatskaya, M. R.; Ghidiu, M.; Gogotsi, Y.; Grey, C. P., NMR Reveals the Surface Functionalisation of Ti3C2 MXene. *Phys. Chem. Chem. Phys.* **2016,** *18* (7), 5099-5102.
33. Persson, P. O.; Rosen, J., Current State of the Art on Tailoring the MXene Composition, Structure, and Surface Chemistry. *Curr. Opin. Solid State Mater. Sci.* **2019,** *23* (6), 100774.
34. Natu, V.; Barsoum, M. W., MXene Surface Terminations: A Perspective. *J. Phys. Chem. C.* **2023,** *127* (41), 20197-20206.
35. Persson, I.; Halim, J.; Lind, H.; Hansen, T. W.; Wagner, J. B.; Näslund, L. Å.; Darakchieva, V.; Palisaitis, J.; Rosen, J.; Persson, P. O., 2D Transition Metal Carbides (MXenes) For Carbon Capture. *Adv. Mater.* **2019,** *31* (2), 1805472.
36. Kamysbayev, V.; Filatov, A. S.; Hu, H.; Rui, X.; Lagunas, F.; Wang, D.; Klie, R. F.; Talapin, D. V., Covalent Surface Modifications and Superconductivity of Two-Dimensional Metal Carbide MXenes. *Science* **2020,** *369* (6506), 979-983.
37. Oschinski, H.; Morales-Garcia, A.; Illas, F., Interaction of First Row Transition Metals with M2C (M= Ti, Zr, Hf, V, Nb, Ta, Cr, Mo, and W) MXenes: A Quest for Single-Atom Catalysts. *J. Phys. Chem. C.* **2021,** *125* (4), 2477-2484.
38. Zhu, S.; Jiang, K.; Chen, B.; Zheng, S., Data-Driven Design of Electrocatalysts: Principle, Progress, and Perspective. *J. Mater. Chem. A.* **2023,** *11* (8), 3849-3870.

39. Ding, K.; Yang, T.; Leung, M. T.; Yang, K.; Cheng, H.; Zeng, M.; Li, B.; Yang, M., Recent Advances in the Data-Driven Development of Emerging Electrocatalysts. *Curr. Opin. Elec.* **2023**, 101404.
40. Umer, M.; Umer, S.; Zafari, M.; Ha, M.; Anand, R.; Hajibabaei, A.; Abbas, A.; Lee, G.; Kim, K. S., Machine Learning Assisted High-Throughput Screening of Transition Metal Single Atom Based Superb Hydrogen Evolution Electrocatalysts. *J. Mater. Chem. A.* **2022,** *10* (12), 6679-6689.
41. Esterhuizen, J. A.; Goldsmith, B. R.; Linic, S., Interpretable Machine Learning for Knowledge Generation in Heterogeneous Catalysis. *Nat. Catal.* **2022,** *5* (3), 175-184.
42. Meng, L.; Yan, L.-K.; Viñes, F.; Illas, F., Effect of Terminations on the Hydrogen Evolution Reaction Mechanism on Ti3C2 MXene. *J. Mater. Chem. A.* **2023,** *11* (13), 6886-6900.
43. Kresse, G.; Furthmüller, J., Efficient Iterative Schemes for Ab Initio Total-Energy Calculations Using a Plane-Wave Basis Set. *Phys. Rev. B.* **1996,** *54* (16), 11169.
44. Kresse, G.; Furthmüller, J., Efficiency of Ab-Initio Total Energy Calculations for Metals and Semiconductors Using a Plane-Wave Basis Set. *Comp. Mater. Sci.s* **1996,** *6* (1), 15-50.
45. Kresse, G.; Hafner, J., Ab Initio Molecular Dynamics for Liquid Metals. *Phys. Rev. B.* **1993,** *47* (1), 558.
46. Perdew, J. P.; Burke, K.; Ernzerhof, M., Generalized Gradient Approximation Made Simple. *Phys. Rev. Lett.* **1996,** *77* (18), 3865.
47. Vega, L.; Vines, F., Generalized Gradient Approximation Adjusted to Transition Metals Properties: Key Roles of Exchange and Local Spin Density. *J. Comp. Chem.* **2020,** *41* (30), 2598-2603.
48. Vázquez-Parga, D.; Fernández-Martínez, A.; Viñes, F., Quantifying the Accuracy of Density Functionals on Transition Metal Bulk and Surface Properties. *J. Chem. Theo. Comp.* **2023,** *19* (22), 8285-8292.
49. Ontiveros, D.; Vela, S.; Viñes, F.; Sousa, C., Tuning MXenes Towards Their Use in Photocatalytic Water Splitting. *Ener. Env. Mater.* **2024,** *7* (6), e12774.
50. Grimme, S.; Antony, J.; Ehrlich, S.; Krieg, H., A Consistent and Accurate Ab Initio Parametrization of Density Functional Dispersion Correction (DFT-D) for the 94 Elements H-Pu. *J. Chem. Phys.* **2010,** *132* (15).
51. Blöchl, P. E., Projector Augmented-Wave Method. *Phys. Rev. B.* **1994,** *50* (24), 17953.
52. Kresse, G.; Joubert, D., From Ultrasoft Pseudopotentials to the Projector Augmented-Wave Method. *Phys. Rev. B.* **1999,** *59* (3), 1758.
53. García-Romeral, N.; Morales-García, Á.; Vines, F.; Moreira, I. d. P.; Illas, F., Theoretical analysis of magnetic coupling in the Ti2C bare MXene. *The Journal of Physical Chemistry C* **2023,** *127* (7), 3706-3714.
54. García-Romeral, N.; Morales-García, Á.; Viñes, F.; de PR Moreira, I.; Illas, F., How Does Thickness Affect Magnetic Coupling in Ti-Based MXenes. *Physical Chemistry Chemical Physics* **2023,** *25* (26), 17116-17127.
55. Bader, R. F., Atoms in Molecules. *Acc. Chem. Res.* **1985,** *18* (1), 9-15.
56. Henkelman, G.; Arnaldsson, A.; Jónsson, H., A Fast and Robust Algorithm for Bader Decomposition of Charge Density. *Comp. Mater. Sci.* **2006,** *36* (3), 354-360.
57. Sanville, E.; Kenny, S. D.; Smith, R.; Henkelman, G., Improved Grid-Based Algorithm for Bader Charge Allocation. *J. Chem. Chem.* **2007,** *28* (5), 899-908.
58. Tang, W.; Sanville, E.; Henkelman, G., A Grid-Based Bader Analysis Algorithm without Lattice Bias. *J. Phys. Cond. Mater.* **2009,** *21* (8), 084204.

59. Di Liberto, G.; Giordano, L.; Pacchioni, G., Predicting the Stability of Single-Atom Catalysts in Electrochemical Reactions. *ACS Catal.* **2023,** *14* (1), 45-55.
60. Pedregosa, F.; Varoquaux, G.; Gramfort, A.; Michel, V.; Thirion, B.; Grisel, O.; Blondel, M.; Prettenhofer, P.; Weiss, R.; Dubourg, V., Scikit-learn: Machine Learning in Python. *J. Machine Learn. Res.* **2011,** *12*, 2825-2830.
61. Manade, M.; Vines, F.; Illas, F., Transition Metal Adatoms on Graphene: A Systematic Density Functional Study. *Carbon* **2015,** *95*, 525-534.
62. Kim, S.; Gamallo, P.; Vines, F.; Lee, J. Y., The Nano Gold Rush: Graphynes as Atomic Sieves for Coinage and Pt-Group Transition Metals. *Appl. Surf. Sci.* **2020,** *499*, 143927.
63. Haynes, W. M., *CRC Handbook of Chemistry and Physics*. CRC press: 2016.
64. Jin, H.; Song, W.; Cao, C., An Overview of Metal Density Effects in Single-Atom Catalysts for Thermal Catalysis. *ACS Catal.* **2023,** *13* (22), 15126-15142.
65. Morales-García, Á.; Mayans-Llorach, M.; Viñes, F.; Illas, F., Thickness Biased Capture of CO_2 on Carbide MXenes. *Phys. Chem. Chem. Phys.* **2019,** *21* (41), 23136-23142.

View Article Online
DOI: 10.1039/D5TA07143G

Data availability

Relevant data are available from the corresponding author upon reasonable request. The data supporting this article have been included as part of the Supplementary Information. The Supplementary Information contains the following contents: adatom adsorption sites, TM-substrate distance before and after H-binding, magnetization value of TM adsorbed on substrate, correlation with DFT-calculated features, parity plot for single variable linear regression models, feature importance analysis for different models, parity plots for different models, leave-one-out experiment with individual metals, comparison of MAE among several models utilizing 10 and 16 features.